Mixed Quantum-Classical Study of Nonadiabatic Dynamics in the $O(^3P_{2,1,0},^1D_2) + H_2$ Reaction

Bin Li and Ke-Li Han*

State Key Laboratory of Molecular Reaction Dynamics, Dalian Institute of Chemical Physics, Chinese Academy of Sciences, Dalian 11602, China

Received: May 20, 2009; Revised Manuscript Received: July 31, 2009

An investigation of the nonadiabatic dynamics for the $O(^3P_{2,1,0},^1D_2) + H_2(v = 0,j = 0)$ reaction is reported using the quantum-classical trajectory method, namely, the coherent switching with decay of mixing (CSDM) theory. The spin−orbit-induced intersystem crossing effects are included by using multiple electronic potential energy surfaces and spin−orbit couplings. The cross sections calculated by the CSDM method are compared with those of a previous exact quantum study, which uses the same potential matrix. The product rotational polarization in nonadiabatic dynamics, including the joint distributions of the angles between the reactant velocity, product velocity, and rotational angular momentum vectors, is presented and compared with the adiabatic results, as well as the vibrational distributions of the products. The influence of spin−orbit coupling is discussed.

I. Introduction

Nonadiabatic coupling effects are involved in many kinds of chemical reactions, and consequently, non-Born−Oppenheimer dynamics has been developed to become more and more effective for investigating the properties of these nonadiabatic reactions.[1−17] Spin−orbit intersystem crossing effects induce nonadiabatic processes in many elementary reactions, and multiple states are involved in the calculation.[18−24] Though many states should be coupled in a nonadiabatic process, the reduced electronic state is adopted in many expressions of nonadiabatic dynamics theory to render the problem tractable. For the $O(^3P_{2,1,0},^1D_2) + H_2(v = 0,j = 0)$ reaction, a quasiclassical trajectory surface hopping (TSH) calculation and an approximate quantum potential (AQP) investigation have been proposed by Schatz and co-workers.[25,26] The $^3A''$ state is a doubly degenerate state, which means that four electronic states $^3A''(1)$, $^3A''(2)$, $^3A'$, and $^1A'$ are involved in the calculation. Also, the quantum wave packet study of this reaction with the same potential energy surfaces (PESs) and spin−orbit couplings has been reported,[1,27] and which provided an accurate branch ratio of the spin state of the product. The quantum calculations for the ground electronic state of the $O(^3P) + H_2$ reaction have also been reported by Balakrishnan[28] and Braunstein et al.[29] From all these investigations, it seems that the spin−orbit coupling effect can be neglected for the total reaction cross sections but is a significant factor in the reactant and product fine-structure resolved cross sections.

The coherent switching with decay of mixing method (CSDM) proposed by Truhlar and co-workers,[30−32] which is derived from the semiclassical Ehrenfest theory (SE)[33−35] and the time-dependent Schrodinger equation in terms of the electronic density matrix, has been validated to be applicable to the two-state nonadiabatic dynamics in our previous work.[36] And we plan to develop this method and algorithm to the multistate nonadiabatic dynamics and the distribution analysis in present study. In the CSDM method, the electronic density matrix varies along with the quasiclassical trajectory propagating on the effective potential which depends on the elements of the density matrix. Since many quantum effects have been taken into account in this theory, the position and probability of nonadiabatic transitions do not have to be measured. Though the four singlet−triplet states of the $O(^3P_{2,1,0},^1D_2) + H_2$ reaction are degenerate in the product region, where the seams of intersection mainly occur, the calculation with the CSDM method avoids a calculation of the nonadiabatic transition probabilities and need not be influenced by the tiny energy gaps between the four PESs. In this work we present a nonadiabatic dynamics investigation of the $O(^3P_{2,1,0},^1D_2) + H_2$ reaction based on the CSDM method for the product spin states $^3\Pi_{3/2}$ and $^3\Pi_{1/2}$, including the cross sections, the product vibrational distributions, and the rotational polarizations involving the spin−orbit coupling. The distributions and polarizations are inaccessibly provided by the full quantum mechanical calculation but useful to understand the physical insight of the scattering tropism and the energy redistribution for the products.

This paper is arranged as follows. In section II, the CSDM theory for nonadiabatic transitions, the formulas of angular momentum polarization, and the PESs and the algorithm used in the calculation are briefly reviewed. Section III presents the results of the calculation, including the branch of cross sections from the three initial ^3P states to the different product spin states, the vibrational distribution of the product, and the joint probability density of the angles between the reactant velocity, product velocity, and rotational angular momentum vector. Concluding remarks and future perspectives are presented in Section IV.

II. Brief Summary of the Theory

A. CSDM Method and the Algorithm. The greatest difference between the CSDM method[32] and previous decay of mixing methods, such as the natural decay of mixing (NDM)[30] and the self-consistent decay of mixing (SCDM),[31] is the probability of switching the decoherent state. While the elements of the electronic density matrix vary along the trajectory by the numerical algorithm for ordinary differential equation, the states are always coherent in the original SE theory.[33−35] In the

* .

10.1021/jp904727d CCC: $40.75
Published on Web 09/01/2009

decay of mixing theory, the derivatives of the electronic density matrix elements, the force, and the derivatives of the PESs would include two terms. One term comes from a fully coherent contribution and the other is a decay-of-mixing part. In the fully coherent contribution, most of the quantum effects are involved, and the density of the electronic wave function will converge to one single decoherent state through the decay-of-mixing term. The choice of decoherent state is determined by the algorithm of the switching probability.

In the CSDM method,[32] the probability of switching the decoherent state for a multistate system is given by

$$P_{\mathrm{K}\rightarrow\mathrm{K}'} = \max\left(-\frac{(b_{\mathrm{K}'\mathrm{K}} - \dot{\tilde{\rho}}_{\mathrm{KK}})\,\mathrm{d}t}{\tilde{\rho}_{\mathrm{KK}}},0\right) \tag{1}$$

where

$$b_{\mathrm{K}'\mathrm{K}} = -2\hbar^{-1}\,\mathrm{Im}(\rho_{\mathrm{K}'\mathrm{K}}U_{\mathrm{K}'\mathrm{K}}) \tag{2}$$

The virtual state populations $\tilde{\rho}_{\mathrm{KK}'}$ evolve following the time-dependent electronic Schrödinger equation,

$$\mathrm{i}\hbar\dot{\tilde{\rho}}_{kk'} = \sum_l (\tilde{\rho}_{lk'}[U_{kl} - \mathrm{i}\hbar\dot{\mathbf{R}}\cdot\mathbf{d}_{kl}] - \tilde{\rho}_{kl}[U_{lk'} - \mathrm{i}\hbar\dot{\mathbf{R}}\cdot\mathbf{d}_{lk'}]) \tag{3}$$

as well as the electronic density matrix elements $\rho_{K'K}$. U_{ij} is the matrix element of the Hamiltonian H_{el}, and $\mathbf{d}_{ij}$ denotes the nonadiabatic coupling vector. The difference between these two sets of populations ($\rho_{\mathrm{K}'\mathrm{K}}$ and $\tilde{\rho}_{\mathrm{KK}'}$) is that the $\tilde{\rho}_{\mathrm{KK}'}$ do not evolve by contributions from the decoherent decay of mixing, which means that the states involved are fully coherent when nonadiabatic coupling is strong. To modify $\tilde{\rho}_{\mathrm{KK}'}$ out of the strong interaction region, the intensity of coupling is defined as[32]

$$D_{\mathrm{K}}(t) = \sum_j |\mathbf{d}_{\mathrm{K}j}|^2 \tag{4}$$

where $\mathbf{d}_{\mathrm{K}j}$ is the nonadiabatic coupling vector and $\tilde{\rho}_{ij}$ should be set equal to ρ_{ij} at each local minimum of $D_{\mathrm{K}}(t)$ along the trajectory. In the CSDM-C method, a component of the nonadiabatic coupling is defined as

$$C_{\mathrm{K}}(t) = \sum_j |\mathbf{d}_{\mathrm{K}j}\cdot\dot{\mathbf{R}}_{\mathrm{vib}}|^2 \tag{5}$$

and is used to modify the virtual state populations instead of $D_{\mathrm{K}}(t)$.

Another benefit is that the CSDM method has been tested to be independent of the representation of the system, shown in ref 32, which means that both the diabatic and adiabatic representations are applicable for the calculation and the results are consistent with each other.[32] In the reaction $\mathrm{O}(^3\mathrm{P}_{2,1,0},^1\mathrm{D}_2) + \mathrm{H}_2$, for the reason that most of the states are degenerate in the product region, the diabatic representation, without using the tiny gap between the two potential surfaces in the denominator to calculate the nonadiabatic coupling vector, works better than the adiabatic representation. Also, if all the properties of the trajectory and population density matrix evolve in the diabatic representation, the conundrum of the final adiabatic product state corresponding to which diabatic state for the degenerate system will also be avoided. Therefore the present investigation is based on the diabatic representation, and the nondiagonal coupling elements U_{ij} are involved in the calculation, instead of the coupling vectors.

In present work, the integral step t_{p} of the phase space (including coordinates and momentums) based on Hamilton's equations, is set to be 0.05 fs. Since the conservation of the state populations ρ_{KK} will be hardly followed in the numerical calculation if the integral step t_{s} of the state population is large, the initial t_s^0 is set to be 10^{-3} fs. When the trajectory propagates into the nonadiabatic coupling region, the integral step t_{s} is alterable and adjusted by the following formula,

$$t_{\mathrm{s}} = \min\left(t_{\mathrm{s}}^0,\left|\frac{A_{\mathrm{err}}}{\dot{\rho}_{kk}}\right|\right) \qquad k = 1-4 \tag{6}$$

where A_{err} is the acceptable error. In the present calculation, A_{err} is 5×10^{-3} to ensure that the change of the state population for each step is less than 5×10^{-3}, which prevents the broken of the state population conservation by low increase of computer time. Other details of the integral program are similar to the previous work.[36]

B. Product Rotational Polarization. In the scattering dynamics, not only the magnitudes of the reactant and product relative velocity vectors (**K**, **K′**) and the product rotational angular momentum **J′**, corresponding to translational and rotational energies, but also the directions of the three vectors are important for understanding the panorama of the reaction.[37−40] The present work refers to two triple-vector correlated angular distributions,

$$P(\theta_{\mathrm{r}},\varphi_{\mathrm{r}}) = \frac{1}{4\pi}\sum_k \sum_{q\geq 0} [a_{q\pm}^k \cos q\varphi_{\mathrm{r}} - a_{q\mp}^k \mathrm{i}\sin q\varphi_{\mathrm{r}}]C_{kq}(\theta_{\mathrm{r}},0) \tag{7}$$

and

$$P(\theta_{\mathrm{t}},\theta_{\mathrm{r}}) = \frac{1}{4}\sum_{k_1k_2} [k_1][k_2]s_{k_20}^{k_1}P_{k_1}(\cos\theta_{\mathrm{t}})\,P_{k_2}(\cos\theta_{\mathrm{r}}) \tag{8}$$

where θ_{t} is the angle between the vectors **K** and **K′**, θ_{r} is the angle between the vectors **K** and **J′**, and ϕ_{r} is the dihedral angle of **K**−**K′**−**J′**. The polarization parameters a_q^k and the coefficients $s_{k_20}^{k_1}$ are evaluated using modified spherical harmonics C_{kq} and Legendre polynomials $P_k(\cos\theta)$, respectively. More details about the product rotational polarization can be found in refs 37−40.

C. Computational Aspects. In the present work, a four-state basis set in the diabatic representation are used to describe the PESs of the $\mathrm{O}(^3\mathrm{P}_{2,1,0},^1\mathrm{D}_2) + \mathrm{H}_2(v = 0, j = 0)$ reaction, as well as the previous TSH and quantum calculations. The potential surface of the single state $^1\mathrm{A}'$ has been described by Dobbyn and Knowles,[41] and those of the triplet states $^3\mathrm{A}''(1)$, $^3\mathrm{A}''(2)$, and $^3\mathrm{A}'$ were reported by Rogers et al.[42] The electronic states $^3\mathrm{A}''(1)$, $^3\mathrm{A}''(2)$, $^3\mathrm{A}'$, and $^1\mathrm{A}'$ correspond to the reactant oxygen states $^3\mathrm{P}_2$, $^3\mathrm{P}_1$, $^3\mathrm{P}_0$, and $^1\mathrm{D}_2$, respectively. The spin−orbit couplings, which are the off-diagonal elements of the Hamiltonian matrix, have been derived from a complete active space self-consistent field (CASSCF) calculation by Hoffmann, Maiti, and Schatz.[26,43] Because not only the values of the nonadiabatic couplings but also their derivatives are required in the semiclas-

sical calculation, the code of the derivatives is evolved from the original program of the couplings by ourselves.

To prevent the integration stepping over local peaks and minima in the switching probabilities, the conventional quasi-classical algorithm, a sixth-order symplectic routine with checked energy conservation and adjustable step length,[44] is employed for the numerical solution in the present work. The CSDM-C method and the anteater procedure is adopted to evolve the decoherent process, which changes the decoherent state only when the switching probability is greater than a random number between 0 and 1. The initial state is chosen as ground vibrational and rotational state ($v = 0$, $j = 0$). Though more trajectories would produce more precise statistics, 10 000−20 000 trajectories were run to calculate the cross section and other properties at each collision energy. It has been proved that the result converges when the sampling number reaches 10^4 or more, through our methodical testing of increasing numbers of trajectories. And more than 60 000 trajectories were run to statistical calculate the angular polarizations of the nonadiabatic transition branches.

III. Results and Discussion

Figure 1 shows the cross sections of different product spin states for the ground rovibrational initial state of H_2 in the collision energy range 6.9−27.7 kcal/mol on the three initial triplet surface $^3A''(1)$,$^3A''(2)$, and $^3A'$. The states $^3A''(1)$ and $^3A''(2)$ correspond to the product OH spin state $\Pi_{3/2}$, and the states $^3A'$ and $^1A'$ can be correlated with the spin state $\Pi_{1/2}$. The calculated CSDM cross sections from the initial state $^3A''(1)$ ($^3P_2$) to the final state $\Pi_{3/2}$ shows noticeable thresholds of ∼12 kcal/mol, as well as that of the final state $\Pi_{1/2}$. Both cross sections, from $^3A''(1)$ to the two final states, increase with the rise of the collision energy. The branch ratio of the product fine-structure $\Pi_{3/2}$ and $\Pi_{1/2}$ is about 12:1 at collision energies higher than 18 kcal/mol but less than 8:1 at lower energies. While the comparative quantum results[27] are also presented in the figure, the cross sections calculated by the CSDM theory are in good agreement with those from quantum theory over the whole range of collision energies, but with a somewhat higher threshold. The next figure of cross sections calculated from the initial state$^3A''(2)$ ($^3P_1$) is quite similar to that of the $^3A''(1)$, since these two triplet states are degenerate on the potential surfaces, with the only difference being the nonadiabatic spin-obit couplings to the rest states $^3A'$ and $^1A'$. However, the final state $\Pi_{1/2}$ branch of the initial state $^3A''(2)$ is a little lower than that of the $^3A''(1)$ state, with a larger branch ratio 25:1 of the product states $\Pi_{3/2}$ and $\Pi_{1/2}$ in the high collision energies region. This property indicates that the transition caused by the spin-obit coupling plays a more important role in the $^3A''(1)$ state than in the $^3A''(2)$ state. In Figure 1c for the $^3A'$ state, the trend of cross sections is the same as those of the Figure 1a,b, though the nonadiabatic transition is more influential than those of the two $^3A''$ states. The branch ratio of the final states $\Pi_{3/2}$ and $\Pi_{1/2}$ is about 1:9 in the high collision energy region. The cross sections of the CSDM method from the initial $^3A'$ state for the two product states both show thresholds of ∼10 kcal/mol, which are quite similar to the quantum results.[27] The difference of cross sections calculated from the initial $^3A'$ state to the product $\Pi_{3/2}$ state by the CSDM method and the quantum mechanism is a little larger than that of the previous states, which means that the effect of the spin−orbit coupling is more or less underestimated in this process. However, most of the present branch cross sections of the three initial triplet states are in good agreement with the results of the quantum

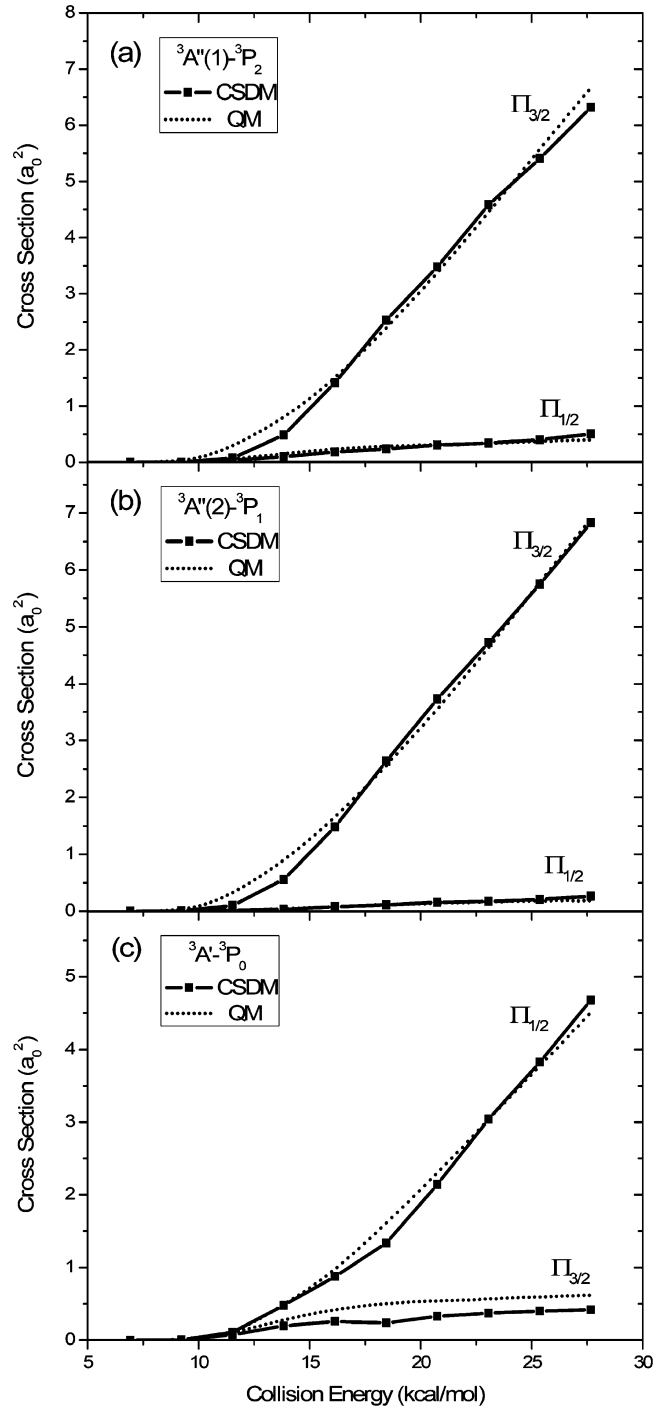

Figure 1. Cross sections of $O(^3P_{2,1,0},{}^1D_2)$ + $H_2(v = 0,j = 0)$ from different initial states to final product states $\Pi_{3/2}$ and $\Pi_{1/2}$ as a function of collision energy in the range 6.9−27.7 kcal/mol, compared with the quantum mechanical results:[27] (a) for initial state $3A''(1)$; (b) for initial state $3A''(2)$; (c) for initial state $3A'$.

mechanism. Thus the CSDM method is used to calculate statistical data for the center-of-mass $\mathbf{K}-\mathbf{K}'-\mathbf{J}'$ angular distributions and the vibrational distributions of the product.

The joint distributions of $P(\theta_r,\phi_r)$ and $P(\theta_t,\theta_r)$ for the initial state $^3A'$ and the different final state ($\Pi_{3/2}$ or $\Pi_{1/2}$) at the collision energy 1.20 eV are shown in Figure 2. All of these results were statistically calculated from the nonadiabatic CSDM trajectories ended in different branches. The angular polarizations of $P(\theta_r,\phi_r)$ for these two branches ($\Pi_{3/2}$ and $\Pi_{1/2}$) both present a strong peak at (90°, 270°), which indicates that the product fragments are ejected with clockwise rotation and the rotational angular

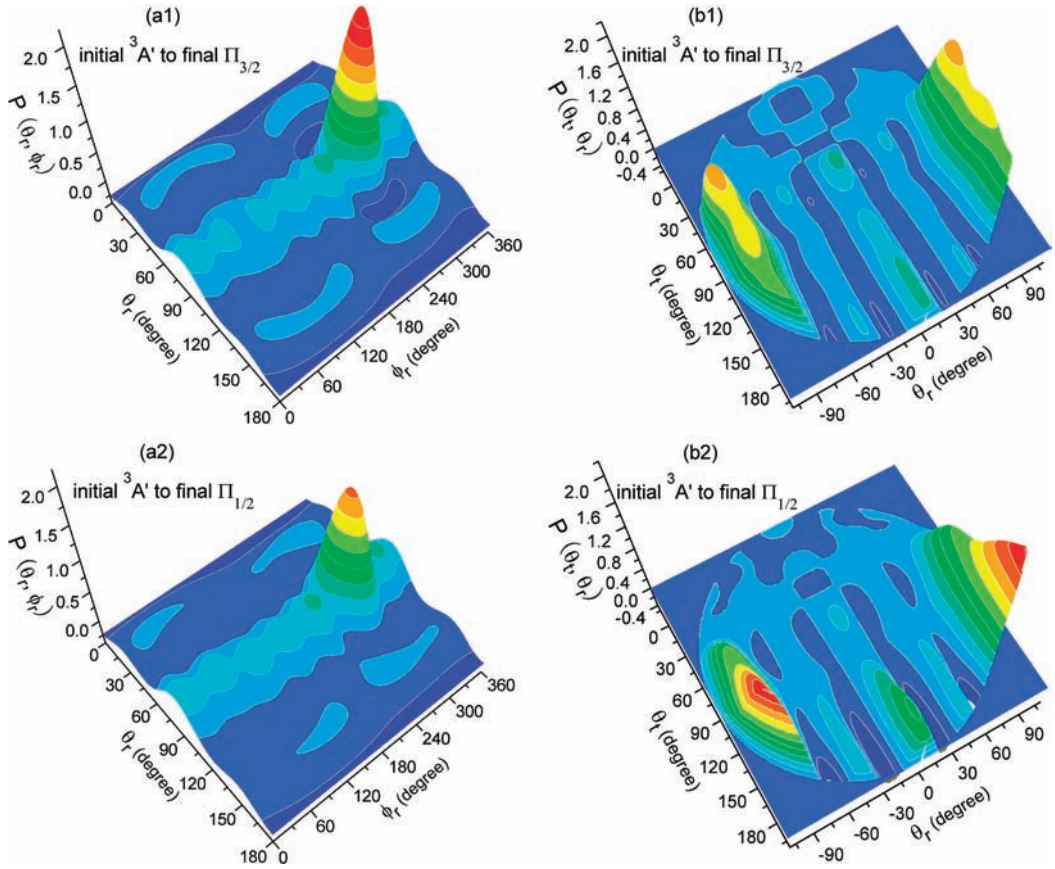

Figure 2. Joint distributions of $P(\theta_r,\phi_r)$ and $P(\theta_t,\theta_r)$ for the initial states $^3A'$ at the collision energy 1.20 eV: (a1, b1) contour maps of $P(\theta_r,\phi_r)$ and $P(\theta_t,\theta_r)$ for the initial state $^3A'$ and final state $\Pi_{3/2}$; (a2, b2) contour maps of $P(\theta_r,\phi_r)$ and $P(\theta_t,\theta_r)$ for the initial state $^3A'$ and final state $\Pi_{1/2}$.

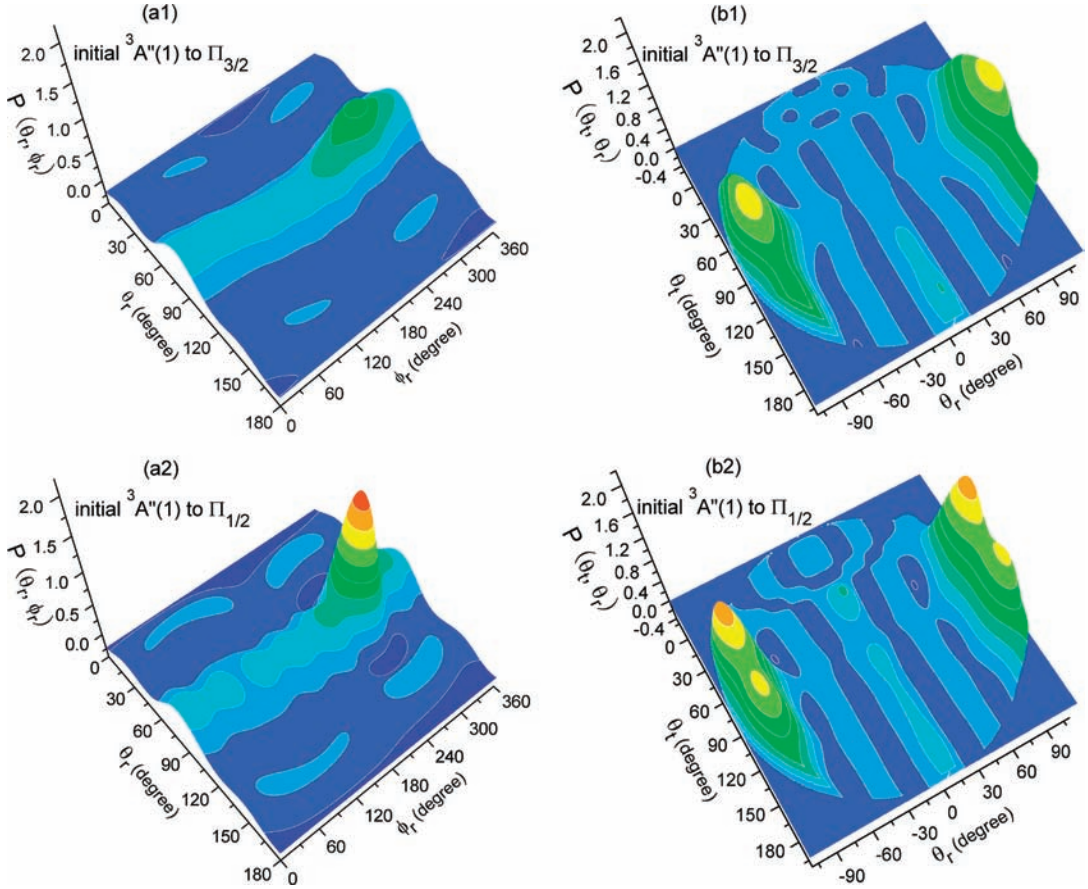

Figure 3. Joint distributions of $P(\theta_r,\phi_r)$ and $P(\theta_t,\theta_r)$ for the initial states $^3A''(1)$ at the collision energy 1.20 eV: (a1, b1) contour maps of $P(\theta_r,\phi_r)$ and $P(\theta_t,\theta_r)$ for the initial state $^3A''(1)$ and final state $\Pi_{3/2}$; (a2, b2) contour maps of $P(\theta_r,\phi_r)$ and $P(\theta_t,\theta_r)$ for the initial state $^3A''(1)$ and final state $\Pi_{1/2}$.

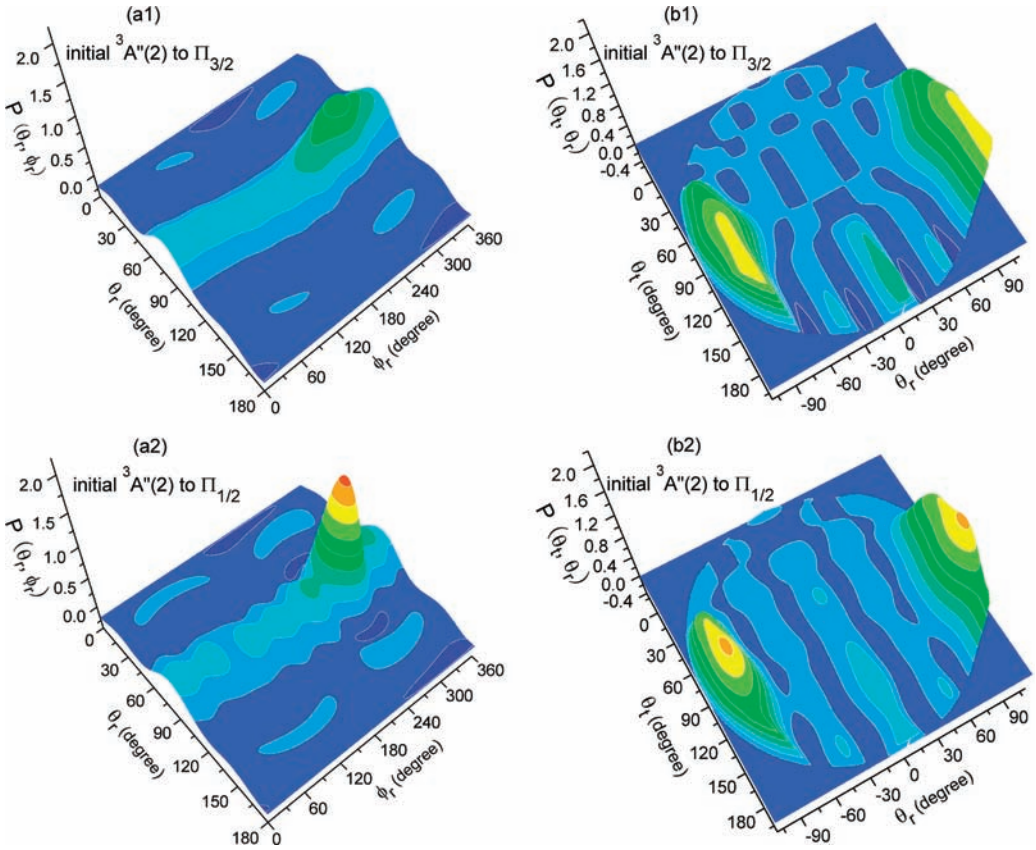

Figure 4. Joint distributions of $P(\theta_r,\phi_r)$ and $P(\theta_t,\theta_r)$ for the initial states $^3A''(2)$at the collision energy 1.20 eV: (a1, b1) contour maps of $P(\theta_r,\phi_r)$ and $P(\theta_t,\theta_r)$ for the initial state $^3A''(2)$ and final state $\Pi_{3/2}$; (a2, b2) contour maps of $P(\theta_r,\phi_r)$ and $P(\theta_t,\theta_r)$ for the initial state $^3A''(2)$ and final state $\Pi_{1/2}$.

momentum is vertical to the reactant-product momentum $\mathbf{K}-\mathbf{K}'$ plane. It can also be concluded from the polarization figure that the plane containing three atoms is reoriented into the K−K′ plane in the reaction process, in spite of the random initial orientation of the reactant molecules. But the peak in map (a1) is higher than that in map (a2), which means that the nonadiabatic transition to the final state $\Pi_{3/2}$ caused by the spin−orbit coupling intensifies the polarization of $P(\theta_r,\phi_r)$. In the maps of $P(\theta_t,\theta_r)$, all peaks are widely distributed and the scattering tropism is not very obvious. However, the vertexes of these peaks are interesting and useful to understand the influence of the spin−orbit couplings for the angler polarization. Two strong peaks appear at (75°, 90°) and (+75°, −90°) in the distributions of $P(\theta_t,\theta_r)$for the final state $\Pi_{3/2}$, while in the map for the final state $\Pi_{1/2}$ the two peaks locate at (150°, 90°) and (+150°, −90°). The different locations of these peaks indicate that product molecules are scattered forward in the original $^3A'$ ($\Pi_{1/2}$) channel, but the scattering direction is changed to backward by the nonadiabatic transition to the $\Pi_{3/2}$ state.

The distributions of $P(\theta_r,\phi_r)$ and $P(\theta_t,\theta_r)$ for the initial states $^3A''(1)$ and the different final state ($\Pi_{3/2}$ or $\Pi_{1/2}$) at a collision energy 1.20 eV are presented in Figure 3. The angular polarizations of $P(\theta_r,\phi_r)$ for these two branches ($\Pi_{3/2}$ and $\Pi_{1/2}$) both present a strong peak at (90°, 270°). But the peak for the $\Pi_{3/2}$ channel is very weak, and that of the $\Pi_{1/2}$ branch is much stronger, which shows an inverse trend in the comparison with Figure 2. It indicates that the nonadiabatic transition to the final state $\Pi_{1/2}$ caused by the spin−orbit coupling also intensifies the polarization of $P(\theta_r,\phi_r)$. In the distributions of $P(\theta_t,\theta_r)$for the final state $\Pi_{3/2}$, the vertexes of two peaks appear at (90°, 90°) and (+90°, −90°), but the locations are changed to (65°, 90°) and (+65°, −90°) in the map of the final state $\Pi_{1/2}$. It can be concluded that the nonadiabatic spin−orbit coupling between the $^3A''(1)$ and $\Pi_{1/2}$ ($^3A'$,$^1A'$) states lead to the more backward scattering direction for this reaction. Figure 4 shows the distributions of $P(\theta_r,\phi_r)$ and $P(\theta_t,\theta_r)$ for the initial states $^3A''(2)$ and the different final state ($\Pi_{3/2}$ or $\Pi_{1/2}$) at a collision energy 1.20 eV. The maps of mdit > $P(\theta_r,\phi_r)$ in Figure 4 are quite similar to those in Figure 3, since the two $^3A''$ states are degenerate, except for the different spin−orbit couplings with the $^3A'$ and $^1A'$ states. The difference of couplings yields that the maps of $P(\theta_t,\theta_r)$ in Figure 4 are different from those in Figure 3. Two peaks present at (150°, 90°) and (+150°, −90°) in the distributions of $P(\theta_t,\theta_r)$ for the final state $\Pi_{3/2}$, and in the map for the $\Pi_{1/2}$ branch the two peaks locate at (110°, 90°) and (+110°, −90°), which means that the nonadiabatic coupling decreases the forward trend of the molecular scattering. The distribution of $P(\theta_t,\theta_r)$ in the $\Pi_{3/2}$ branch in Figure 4 is a little different with that in Figure 3, though the two $^3A''$ states are degenerate. This property indicates that all of the trajectories are influenced by the nonadiabatic coupling, though most of them do not finally transit to the product state $\Pi_{1/2}$, and this difference between the spin−orbit couplings yields the little difference between these angular polarization of the two degenerate states. Thus it can be concluded that the spin−orbit coupling plays a more important role in the angular polarization $P(\theta_t,\theta_r)$ of the two triplet states.

Figure 5 presents the vibrational distributions of the product OH for the states $^3A''(1)$, $^3A''(2)$, and $^3A'$ in both adiabatic and nonadiabatic dynamics. All of these results were also calculated by the CSDM method based on the four surfaces system, i.e., three triplet states and one singlet state. Since the $^3A''(1)$ and $^3A''(2)$ states are degenerate in the adiabatic representation, we compare the two nonadiabatic dynamics results with one

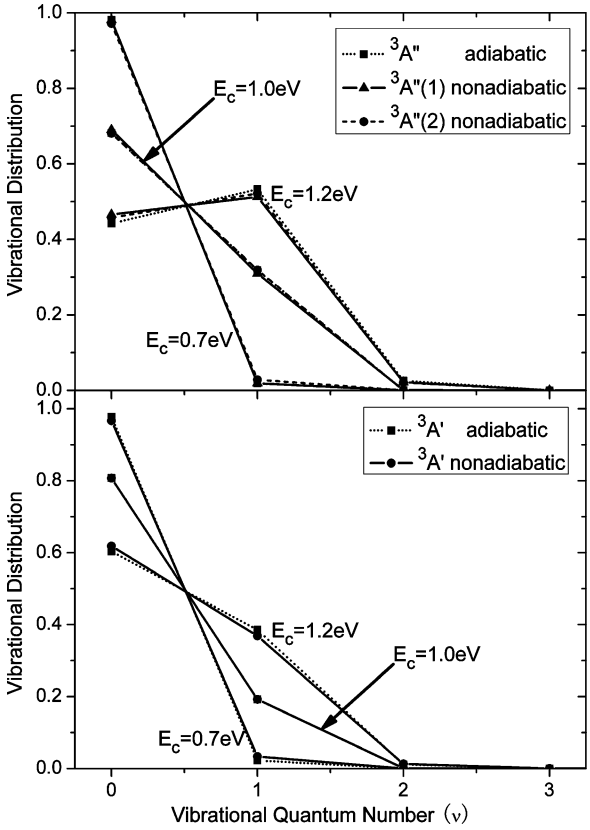

Figure 5. Vibrational distributions of the product OH for the initial states $^3A''(1)$, $^3A''(2)$, and $^3A'$ of $O(^3P_{2,1,0},^1D_2) + H_2(v = 0,j = 0)$ at the collision energies of 0.7, 1.0, and 1.2 eV.

adiabatic results, $^3A''$. It is obvious that the distributions of the vibrational state $v = 1$ or higher vibrational numbers increase along with the rise of the collision energy, for all of the triplet states. The increase of the high vibrational distribution for the state $^3A'$ is less pronounced than that for the states $^3A''(1)$ and $^3A''(2)$, referring to the higher energy barrier in the state $^3A'$. These plots also show that the effect of the nonadiabatic spin−orbit coupling is negligible, especially at low collision energy, but more noticeable at high collision energy. The nonadiabatic coupling slightly decreases the excitation of the vibrational state of the product OH for all three states, which indicates that the nonadiabatic transition consumes part of the products' vibrational energy. This phenomenon also corresponds to the arguments found in the previous work of Marti and Schatz,[26] in which they state that the nonadiabatic transitions mostly take place in the product channel. The low transition probability of this system makes the influence of the spin−orbit coupling on the distributions not very considerable.

The present study of the angular polarization and the vibrational distribution shows some interesting properties of this reaction. We know that the energy barrier on the reaction coordinate of the $^3A'$ state is higher than that of the $^3A''$ state,[45] and the angular distributions of $^3A'$ in Figure 2 are generally higher than those of $^3A''$ in Figures 3 and 4, indicating that the rotational angular momentum is *naturally* vertical to the reactant-product momentum $\mathbf{K}-\mathbf{K}'$ plane with a clockwise direction for the $O + H_2$ reaction on these triplet states; also, the higher energy barrier would strengthen the angular polarization. From the comparison of the vibrational distributions for the $^3A''$ and $^3A'$ states, it can be found that the higher energy barrier bate the excitation of the product vibrational state. The influence of the spin−orbit coupling on the angular polarization is considerable.

IV. Conclusion

The nonadiabatic dynamics of the multistate reaction system of $O(^3P_{2,1,0},^1D_2) + H_2(v = 0,j = 0)$ has been investigated by the CSDM method. All the calculations are based on the four-state surfaces system in the diabatic representation. Since the potential surfaces are degenerate in the product region, the consistency with the quantum results can be developed by the CSDM method, which avoids any calculation of the transition probability and position. A comparison of the branch cross sections from the quantum mechanism and the present decay of mixing theory indicates that this method yields encouraging results for a nonadiabatic reaction with spin−orbit coupling effects. The joint distributions of the angles between the reactant velocity, product velocity, and rotational angular momentum vectors are shown to exhibit a product rotational polarization effect in the scattering process of the reaction. And the vibrational distributions of the product express the influence of the collision energy and the reorganization of the vibrational energy. It is also found that the nonadiabatic spin−orbit coupling effect plays a role in most of these results, changing more or less the distributions of angles and vibrational states. Our future work will focus on more complex systems, such as the nonadiabatic dynamics of a multistate organic compound or a materials surface model.

References and Notes

(1) Chu, T. S.; Zhang, Y.; Han, K. L. *Int. Rev. Phys. Chem.* **2006**, *25*, 201.
(2) Blais, N. C.; Truhlar, D. G. *J. Chem. Phys.* **1983**, *79*, 1334.
(3) Stine, J. R.; Muckerman, J. T. *J. Phys. Chem.* **1987**, *91*, 459.
(4) Tully, J. C. *J. Chem. Phys.* **1990**, *93*, 1061.
(5) Kuntz, P. J. *J. Chem. Phys.* **1991**, *95*, 141.
(6) Hammes-Schiffer, S.; Tully, J. C. *J. Chem. Phys.* **1994**, *101*, 4657.
(7) Zhu, C.; Nakamura, H. *J. Chem. Phys.* **1994**, *101*, 10630.
(8) Zor, D.; Kay, K. G. *Phys. Rev. Lett.* **1996**, *76*, 1990.
(9) Sun, X.; Miller, W. H. *J. Chem. Phys.* **1997**, *106*, 916.
(10) Müller, U.; Stock, G. *J. Chem. Phys.* **1997**, *107*, 6230.
(11) Volobuev, Y. L.; Hack, M. D.; Truhlar, D. G. *J. Phys. Chem. A* **1999**, *103*, 6225.
(12) Hack, M. D.; Jasper, A. W.; Volobuev, Y. L.; Schwenke, D. W.; Truhlar, D. G. *J. Phys. Chem. A* **1999**, *103*, 6309.
(13) Takayanagi, T.; Kurosaki, Y.; Ichihara, A. *J. Chem. Phys.* **2000**, *112*, 2615.
(14) Volobuev, Y. L.; Hack, M. D.; Topaler, M. S.; Truhlar, D. G. *J. Chem. Phys.* **2000**, *112*, 9716.
(15) Elran, Y.; Kay, K. G. *J. Chem. Phys.* **2001**, *114*, 4362.
(16) Zhu, C.; Kamisaka, H.; Nakamura, H. *J. Chem. Phys.* **2002**, *116*, 3234.
(17) Oloyede, P.; Mil'nikov, G.; Nakamura, H. *J. Chem. Phys.* **2006**, *124*, 144110.
(18) Alexander, M. H.; Manolopoulos, D. E.; Werner, H. J. *J. Chem. Phys.* **2000**, *113*, 11084.
(19) Hoffmann, M. R.; Schatz, G. C. *J. Chem. Phys.* **2000**, *113*, 9456.
(20) Zhang, Y.; Xie, T. X.; Han, K. L.; Zhang, J. Z. H. *J. Chem. Phys.* **2003**, *119*, 12921.
(21) Schatz, G. C.; Hankel, M. T.; Whiteley, W. J.; Connor, J. N. L. *J. Phys. Chem. A* **2003**, *107*, 7278.
(22) Balucani, N.; Skouteris, D.; Cartechini, L.; Capozza, G.; Segoloni, E.; Casavecchia, P.; Alexander, M. H.; Capecchi, G.; Werner, H.-J. *Phys. Rev. Lett.* **2003**, *91*, 013201.
(23) Zhang, Y.; Xie, T. X.; Han, K. L.; Zhang, J. Z. H. *J. Chem. Phys.* **2004**, *120*, 6000.
(24) Tang, K. C.; Liu, K. L.; Chen, I. C. *Chem. Phys. Lett.* **2004**, *386*, 437.
(25) Hoffmann, M. R.; Schatz, G. C. *ACS Symp. Ser.* **2002**, *828*, 329.
(26) Maiti, B.; Schatz, G. C. *J. Chem. Phys.* **2003**, *119*, 12360.
(27) Chu, T. S.; Zhang, X.; Han, K. L. *J. Chem. Phys.* **2005**, *122*, 214301.
(28) Balakrishnan, N. *J. Chem. Phys.* **2004**, *121*, 6346.
(29) Braunstein, M.; Adler-Golden, S.; Maiti, B.; Schatz, G. C. *J. Chem. Phys.* **2004**, *120*, 4316.
(30) Hack, M. D.; Truhlar, D. G. *J. Chem. Phys.* **2001**, *114*, 9305.
(31) Zhu, C.; Jasper, A. W.; Truhlar, D. G. *J. Chem. Phys.* **2004**, *120*, 5543.

(32) Zhu, C.; Nangia, S.; Jasper, A. W.; Truhlar, D. G. *J. Chem. Phys.* **2004**, *121*, 7658. Cheng, S. C.; Zhu, C.; Liang, K. K.; Lin, S. H.; Truhlar, D. G. *J. Chem. Phys.* **2008**, *129*, 024112.
(33) Meyer, H. D.; Miller, W. H. *J. Chem. Phys.* **1979**, *70*, 3214.
(34) Micha, D. A. *J. Chem. Phys.* **1983**, *78*, 7138.
(35) García-Vela, A.; Gerber, R. B.; Imre, D. G. *J. Chem. Phys.* **1992**, *97*, 7242.
(36) Li, B.; Chu, T. S.; Han, K. L. *J. Comput. Chem.* in press.
(37) Aoiz, F. J.; Brouard, M.; Enriquez, P. A. *J. Chem. Phys.* **1996**, *105*, 4964.
(38) Wang, M. L.; Han, K. L.; He, G. Z. *J. Phys. Chem. A* **1998**, *102*, 10204.
(39) Han, K. L.; He, G. Z.; Lou, N. Q. *J. Chem. Phys.* **1996**, *105*, 8699.
(40) Wang, M. L.; Han, K. L.; He, G. Z. *J. Chem. Phys.* **1998**, *109*, 5446.
(41) Dobbyn, J.; Knowles, P. J. *Faraday Discuss.* **1998**, *110*, 247.
(42) Rogers, S.; Wang, D.; Kuppermann, A.; Walch, S. *J. Phys. Chem. A* **2000**, *104*, 2308.
(43) Hoffmann, M. R.; Schatz, G. C. *J. Chem. Phys.* **2000**, *113*, 9456.
(44) Zhang, X.; Han, K. L. *Int. Quantum Chem.* **2006**, *106*, 1815.
(45) Garashchuk, S.; Rassolov, V. A.; Schatz, G. C. *J. Chem. Phys.* **2006**, *124*, 244307.

JP904727D